ACS OMEGA

Open Access

http://pubs.acs.org/journal/acsodf

Article

Unveiling Structural Variations in Armchair-Edge Coronoids by Spectroscopies

Jungpil Kim*

Cite This: *ACS Omega* 2024, 9, 43956−43962

Read Online

ACCESS | Metrics & More | Article Recommendations | Supporting Information

ABSTRACT: This study explores the electronic and vibrational properties of armchair coronoids (ACs), a unique class of polycyclic aromatic hydrocarbons with varying molecular and cavity sizes. Through density functional theory simulations, we investigated the X-ray photoelectron spectroscopy (XPS) and Raman spectra of C222, C114, C42, and their derivatives with different cavity sizes. The results reveal that band gaps and electronic properties of ACs can be precisely tuned by adjusting the molecular and cavity dimensions. XPS spectra demonstrated shifts in binding energy correlating with bandgap variations, while Raman spectra exhibited distinct C−C stretching and breathing modes. Notably, the introduction of cavities led to shifts in the breathing mode band, providing insights into the structural identification of ACs through Raman spectroscopy. The findings suggest that combining XPS and Raman spectroscopy can effectively characterize ACs, offering a comprehensive understanding of their structure−property relationships. This research lays the groundwork for future experimental and theoretical studies on the potential applications of ACs in electronic materials.

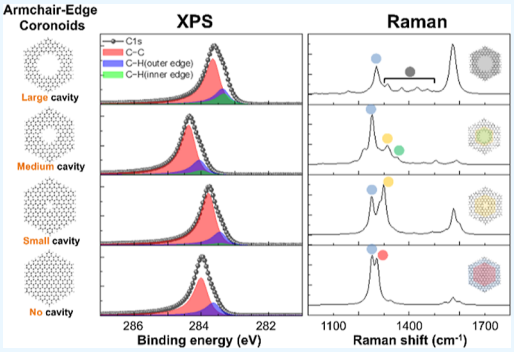

INTRODUCTION

Coronoids, a distinct class of polycyclic aromatic hydrocarbons, are characterized by their cyclic structures, where multiple benzene rings are fused to create a closed-loop with a central cavity.[1,2] The electronic properties of coronoids are largely determined by their bandgap, which can be precisely adjusted by varying both the molecular size and cavity dimensions, positioning them as promising candidates for next-generation electronic materials.[1−4] Unlike graphene, which features delocalized π-electrons across its entire structure, coronoids exhibit localized π-electrons that are accurately represented by Clar's model.[5] Since the initial synthesis of coronoids such as kekulene by Staab and Diederich in 1978,[6] numerous coronoids such as cyclo[d,e,d,e,e,d,e,d,e,e]decakisbenzene,[7] septulene,[8] octulene,[9] and extended C216 coronoids[10] have been successfully synthesized, and their electronic properties have been comprehensively studied in relation to their structural features (Figure 1a).[1,11,12]

Coronoids can be classified into armchair and zigzag-edged variants depending on their edge morphology, and these edge structures play a pivotal role in defining their electronic characteristics.[5,13] Zigzag-edged coronoids (ZCs) exhibit magnetic properties due to unpaired electrons at the edges, whereas armchair coronoids (ACs) typically lack significant magnetic characteristics.[14] However, the armchair edge configuration is less chemically reactive compared to the zigzag edge, which renders ACs more suitable for stable electronic applications.[15]

The electronic structure of ACs is significantly influenced by both molecular size and cavity size, necessitating detailed structural analysis of these parameters to effectively leverage their properties for practical applications.[1,2,16] Microscopic techniques such as scanning tunneling microscopy and atomic force microscopy have primarily been used for direct structural observation of ACs.[1,16,17] Additionally, analyses employing infrared spectroscopy, nuclear magnetic resonance, Raman spectroscopy, UV−visible spectroscopy, and secondary ion mass spectrometry have also been reported.[1,10,12] Microscopy provides the benefit of direct structural visualization, but its limitations in evaluating entire samples require the use of complementary spectroscopic methods. To the best of our knowledge, X-ray photoelectron spectroscopy (XPS), a widely used analytical technique for carbon materials, has not yet been reported. Although Raman spectroscopy has been performed on certain structures,[10,12] detailed studies on variations in Raman spectra with respect to molecular and cavity sizes remain limited. Assessing XPS and Raman spectra based on these parameters requires the synthesis of various samples for comparative analysis, presenting challenges for experimental approaches. Our

Received: August 29, 2024
Revised: October 3, 2024
Accepted: October 9, 2024
Published: October 15, 2024

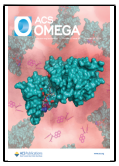

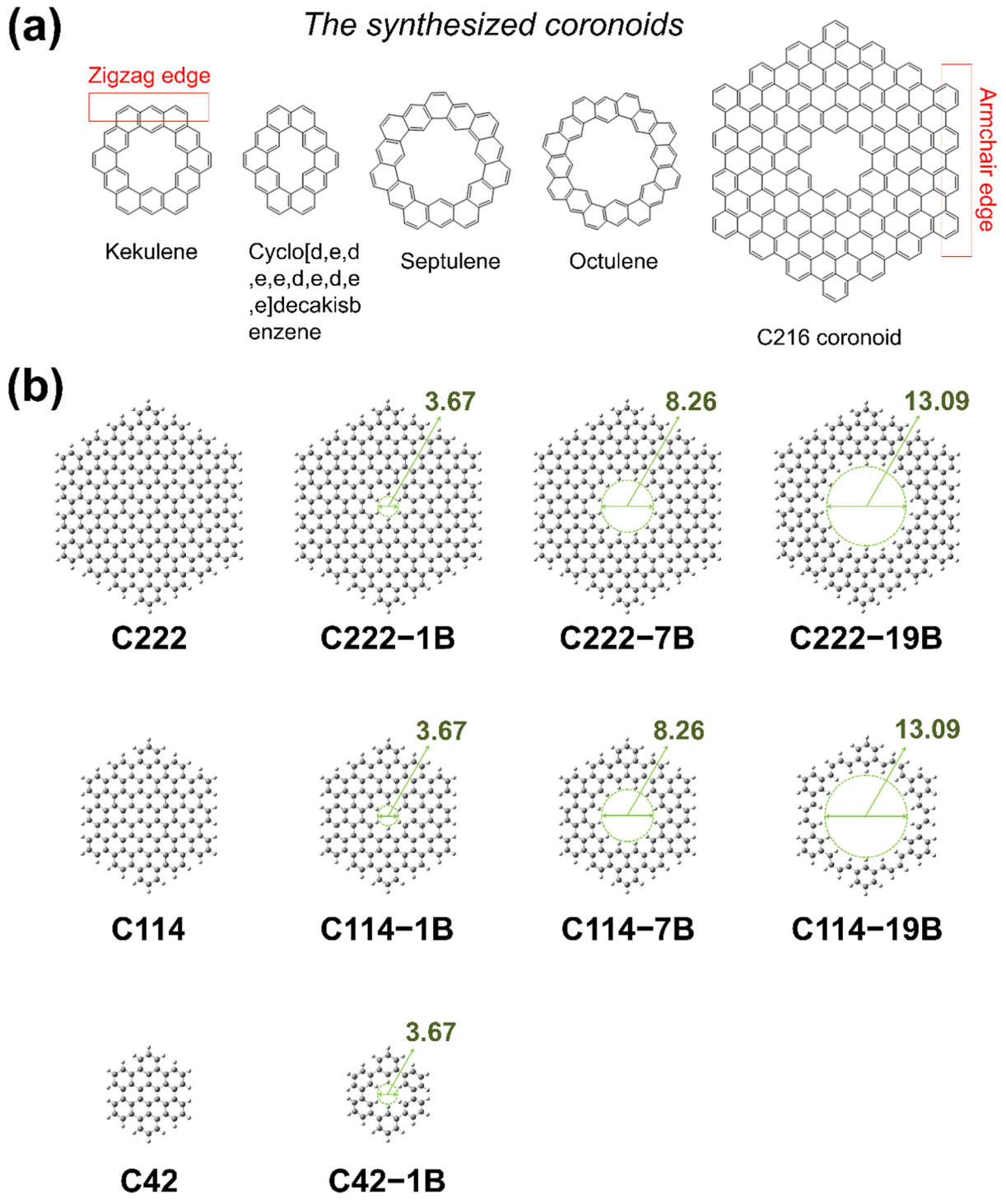

Figure 1. (a) Representative synthetic achievements of coronoids. (b) Optimized structures of C222, C114, C42, and the coronoids derived from these structures calculated in this work. The values correspond to the distances (Å) between two atoms.

group has previously reported that simulated XPS and Raman spectra, derived from the atomic structures of nanocarbon materials, closely match experimental data. This method has been effectively applied to the analysis of pentagons,[18,19] heptagons,[18,20] vacancies,[21] and both zigzag and armchair edges of nanocarbons,[22,23] as well as ZCs,[4] suggesting that simulations can also be effectively applied to the study of ACs.

In this study, cavities of various sizes were introduced into $C_{222}H_{40}$, $C_{114}H_{30}$, and $C_{42}H_{18}$, followed by simulated XPS and Raman spectroscopy (Figure 1). Shifts in the XPS spectra were observed in relation to changes in bandgap, and the characteristic bands in the Raman spectra were assigned based on molecular and cavity sizes. This research is anticipated to lay a foundation for future XPS and Raman analyses of synthesized AC samples.

RESULTS AND DISCUSSION

Figure 1 presents the optimized configurations of C222, C114, and C42 molecules, along with the ACs featuring various cavity sizes incorporated into these structures. The pores were created

https://doi.org/10.1021/acsomega.4c07966
ACS Omega 2024, 9, 43956−43962

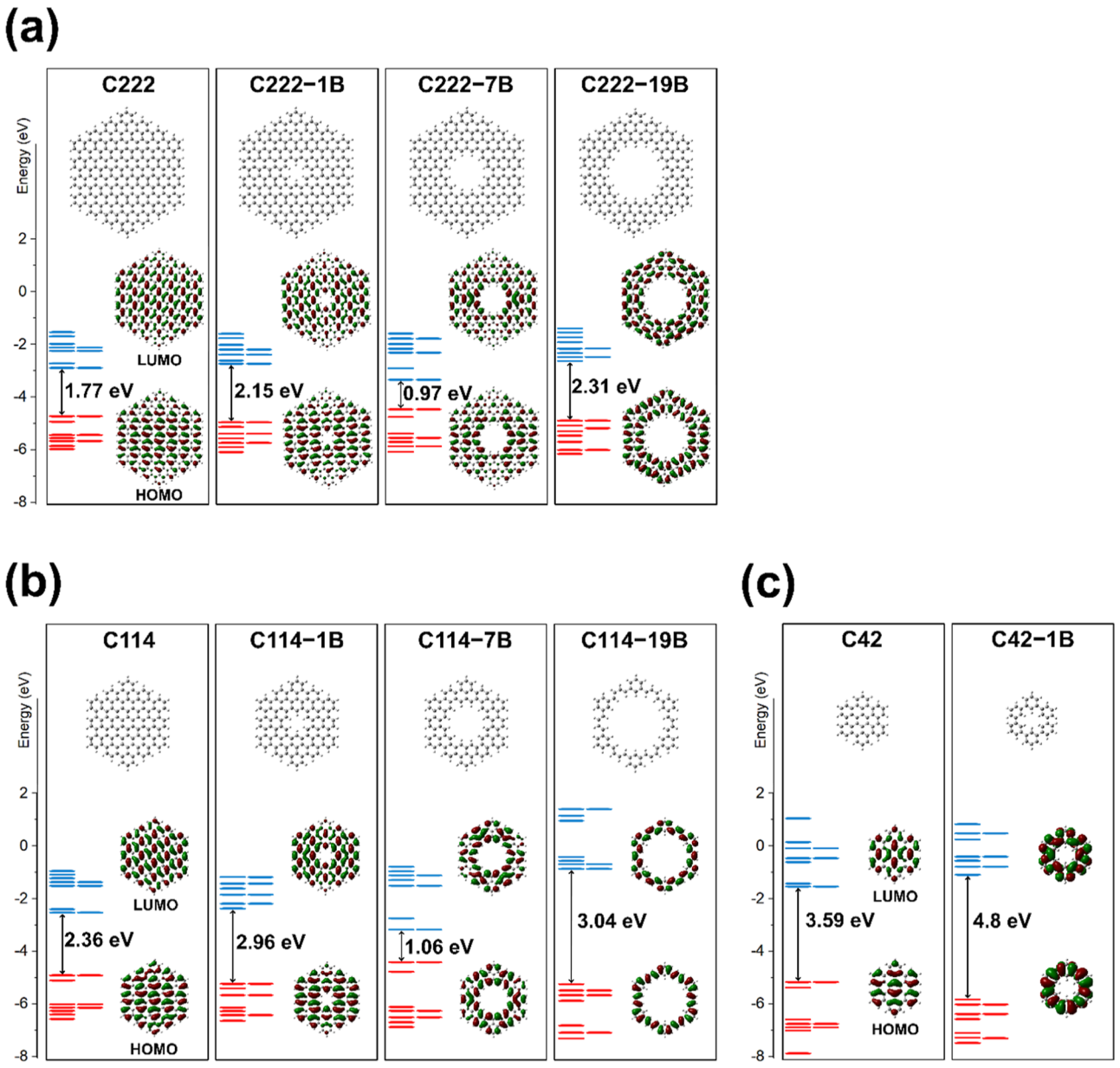

Figure 2. Energies and states of the HOMO and LUMO for the (a) *C*222−*n*Bs, (b) C114−*n*Bs, and (c) C42−*n*Bs.

by extracting 1, 7, and 19 benzene rings (B) from the central region of the molecules, resulting in pore diameters of 3.67, 8.26, and 13.09 Å for the −1B, −7B, and −19B configurations, respectively (Figure 1b). For instance, the *C*222−19B structure corresponds to a *C*222 molecule with 19 benzene rings removed, yielding a pore diameter of 13.09 Å.

In *C*222, C114, and C42 without cavities, the band gaps are 1.78, 2.38, and 3.59 eV, respectively (Figure 2). It is evident that the band gap increases as the molecular size decreases due to the reduction in the π-conjugated structure.[24,25] Generally, introducing cavities into graphene leads to an increase in band gaps.[26] This phenomenon has been observed in coronoids, a localized region of graphene, where the effect on the band gap varies depending on the edge type. In ZCs, the band gap either decreases or increases depending on the size of the cavity.[4,13,27] For instance, for ZCs with an even number of carbon atoms (NC) between the inner and outer edges, the band gap increases, whereas for those with an odd NC, the band gap decreases.[4] However, in ACs, the band gap consistently increases with larger cavities.[1] For example, Giovannantonio et al. demonstrated that the band gaps of *C*222, *C*222−1B, and *C*222−19B ACs are 1.77, 2.15, and 2.25 eV, respectively, indicating a proportional relationship between cavity size and band gap.[1]

To further explore this trend, we calculated the band gap of *C*222−7B. The band gaps of *C*222, *C*222−1B, *C*222−7B, and *C*222−19B are 1.78, 2.16, 0.98, and 2.35 eV, respectively, showing that the relationship between cavity size and band gap is not always linear (Figure 2a). Notably, in specific structures such as *C*222−7B, the band gap is the lowest. This trend is similarly observed in the C114−*n*B series, where the band gap of C114−7B is the lowest at 1.06 eV (Figure 2b). This is because the highest occupied molecular orbital (HOMO) and lowest unoccupied molecular orbital (LUMO) orbitals are highly similar in the −7B configuration, sharing the same symmetry (Figure 2a,b), which allows electrons to be easily excited from

https://doi.org/10.1021/acsomega.4c07966
ACS Omega 2024, 9, 43956−43962

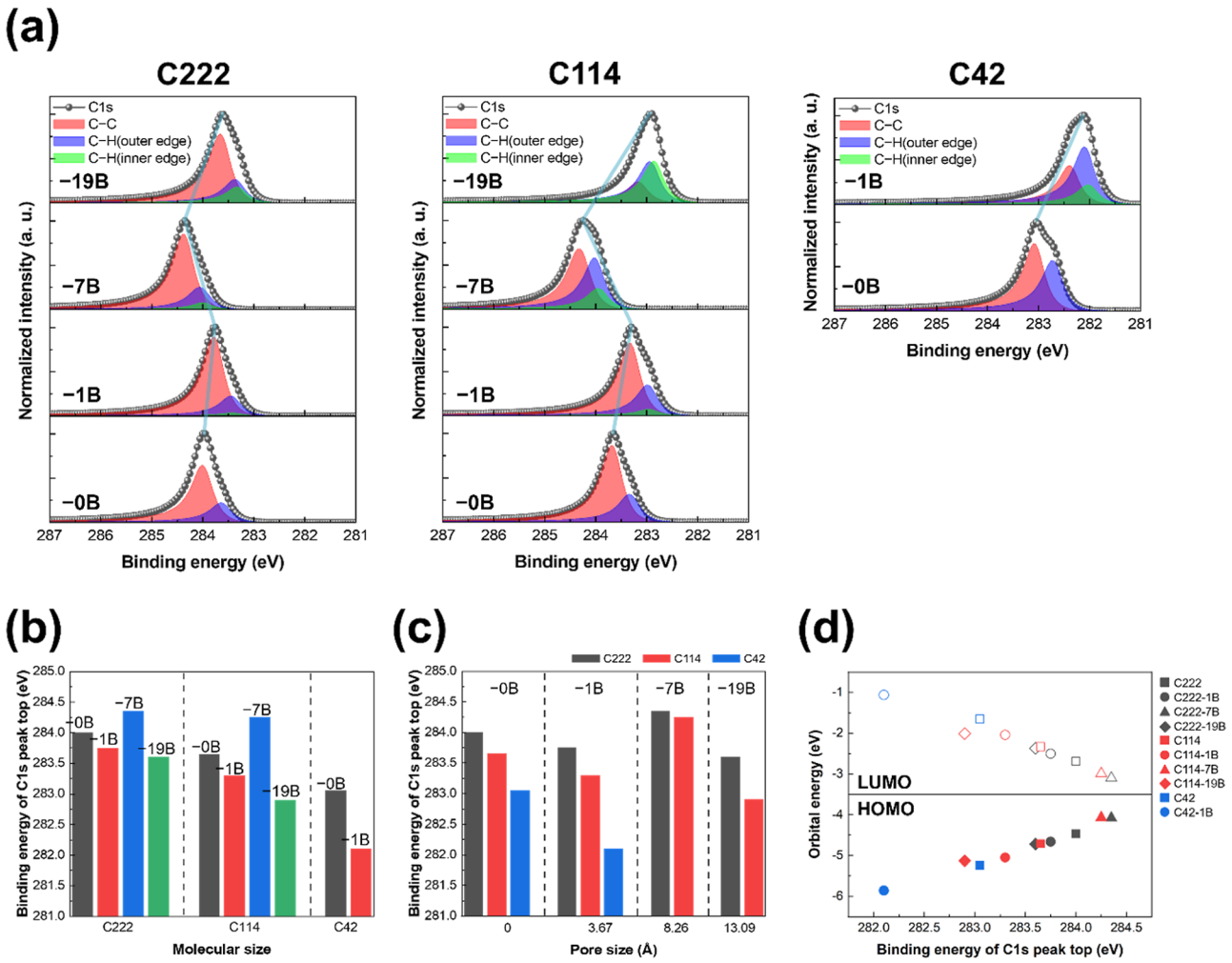

Figure 3. Simulated C 1s XPS analysis. (a) C 1s XPS spectra for all structures. Original spectra (black dotted line) are separated into three peaks corresponding to C−C (red region), C−H on outer edges (purple region), and C−H on inner edges (green region). Relationship between C 1s peak position and (b) molecular size, (c) pore size, and (d) HOMO and LUMO energies.

Table 1. Peaks of C 1s Spectra and the Energies of HOMO and LUMO for All Structures

	peak top (eV)				orbital energy (eV)		
structure	C 1s	C−C	C−H (outer edge)	C−H (inner edge)	HOMO	LUMO	band gap
*C*222	284.0	284.0	283.7	–	−4.47	−2.69	1.78
*C*222−1B	283.8	283.8	283.5	283.5	−4.66	−2.50	2.16
*C*222−7B	284.4	284.4	284.1	284.0	−4.08	−3.10	0.98
*C*222−19B	283.6	283.7	283.4	283.3	−4.72	−2.37	2.35
C114	283.7	283.7	283.4	–	−4.71	−2.33	2.38
C114−1B	283.3	283.4	283.0	283.0	−5.05	−2.04	3.01
C114−7B	284.3	284.3	284.0	284.0	−4.07	−2.99	1.08
C114−19B	282.9	283.2	283.0	282.9	−5.13	−2.01	3.12
C42	283.1	283.1	282.7	–	−5.24	−1.65	3.59
C42−1B	282.1	282.4	282.1	282.1	−5.86	−1.06	4.80

the HOMO to the LUMO.[28] The variation in the band gap of nanocarbon materials is a crucial factor in determining the peak position of the C 1s XPS spectra,[4,18−24] indicating that the ACs can be analyzed based on the C 1s XPS peak position, as their band gaps vary according to their structure.

Figure 3 shows the C 1s spectra (Figure 3a) and the peak positions of the C 1s spectra in relation to molecular size (Figure 3b), pore size (Figure 3c), and bandgap (Figure 3d) for the structures depicted in Figure 1. For *C*222, C114, and C42 without cavities, as the molecular size decreased, the HOMO energy also decreased, leading to a reduction in the binding energy (BE) between the HOMO and C 1s core level, which resulted in the C 1s peaks shifting to lower BE values (Figure 3d and Table 1).[18] Consequently, the C 1s peaks for *C*222, C114, and C42 were located at 284.0, 283.7, and 283.1 eV, respectively.

The C 1s spectra of these cavity-free structures can be resolved into two distinct peaks: C−C and C−H (outer edge) (Figures 1 and 3a). The C−H (outer edge) peak was generally

https://doi.org/10.1021/acsomega.4c07966
ACS Omega 2024, 9, 43956−43962

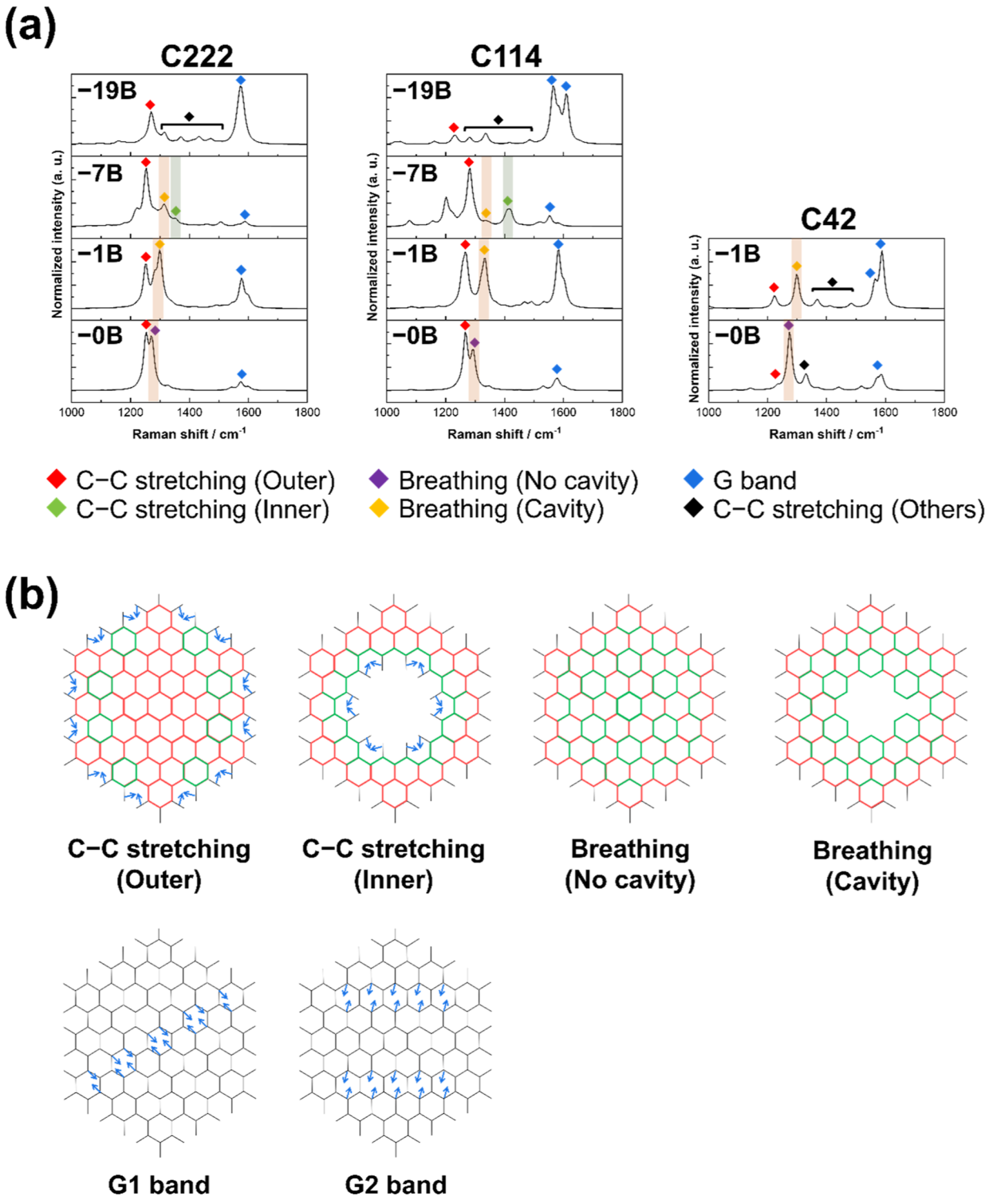

Figure 4. Raman spectra and vibrational modes of the ACs. (a) Raman spectra of ACs. (b) Vibrational modes for characteristic bands of the Raman spectra shown in Figure 4a.

observed at a BE of 0.3 eV lower than the C−C peak, due to the electron-donating effect of the hydrogen atom in C−H (outer edge) which increases the electron density on the carbon atom.[4,18−24] For ACs with cavities, the C 1s spectra included an additional peak for C−H (inner edge), alongside the C−C and C−H (outer edge) peaks (Figure 3a), reflecting similar C−H bonding characteristics. However, the BE of the C−H (inner edge) peak was typically 0.1 eV lower than that of the C−H (outer edge) peak, indicating that the carbon atoms in the inner edge C−H bonds possess higher electron density than those in the outer edge C−H bonds.[4] Since all the structures calculated in this study are composed solely of C−C and C−H bonds, the full width at half-maximum values were small, ranging from 0.7 to 0.75 eV, and there were no significant differences between the structures.

https://doi.org/10.1021/acsomega.4c07966
ACS Omega 2024, 9, 43956−43962

The C 1s peaks for the *C*222−*n*B structures were positioned between 283.6 and 284.4 eV, for C114−*n*B between 282.9 and 284.3 eV, and for C42−*n*B between 282.1 and 283.1 eV (Figure 3 and Table 1). For structures of same molecular size, such as the *C*222−*n*B and C114−*n*B series (Figure 3a,b and Table 1), the C 1s peaks for *C*222−7B and C114−7B, which have smaller bandgaps, shifted up to 0.4 eV higher in BE compared to the C 1s peaks of *C*222 and C114, respectively. On the other hand, the C 1s peaks for ACs with larger bandgaps, such as those in the −1B and −19B structures, shifted up to 1.0 eV lower in BE. For structures with the same pore size (Figure 3a,c and Table 1), differences in molecular size could be identified based on the peak positions, except in the −7B structures with a pore size of 8.26 Å, where the peak positions of *C*222−7B and C114−7B differed by only 0.1 eV. However, in the −1B structures with a pore size of 3.67 Å, the C42−1B peak shifted 1.7 eV lower than that of *C*222−1B. Similarly, in the −19B structures with a pore size of 13.09 Å, the peaks of *C*222−19B and C114−19B exhibited a significant difference of 0.7 eV. It implies that the unknown sample can be analyzed using the difference in peak positions of these samples. However, due to the limitations of XPS in providing a comprehensive analysis of ACs, it is necessary to complement it with other techniques, such as Raman spectroscopy, for more accurate analysis.

The molecular dimensions and edge structures of 2D nanocarbon materials, such as ACs, have a significant impact on the D (1150−1450 cm^{-1}) and G (1500−1600 cm^{-1}) band regions in their Raman spectra.[4,12,18] Consequently, the Raman shift range between 1000−1800 cm^{-1} was thoroughly estimated (Figure 4a). The Raman spectra covering the full range of 0−4000 cm^{-1} are presented in Figure S4, with detailed band assignments provided in the Supporting Video and Table S1. The distinct Raman bands of ACs are attributed to C−C stretching, breathing, and G band vibrations (Figure 4 and Supporting Video). The typical C−C stretching and breathing modes are categorized into four types based on the presence or absence of cavities (Figure 4b and Supporting Video): (1) C−C stretching at the outer edges (1224−1280 cm^{-1}); (2) C−C stretching at the inner edges (1354−1410 cm^{-1}); (3) breathing mode without a cavity (1273−1293 cm^{-1}); and (4) breathing mode with a cavity (1299−1334 cm^{-1}).[12] Additional C−C stretching modes are observed as several bands within the 1250−1500 cm^{-1} region.

The C−C stretching (outer) and breathing (No cavity) modes in the *C*222, C114, and C42 structures without cavities originate from the stretching of Clar rings and closely resemble the phonon patterns observed at the *K* wave vector in graphene.[12] Additionally, the C−C stretching (Outer) mode significantly contributes to the C−H vibrations at the edges, while the breathing (No cavity) mode exhibits stronger vibrations toward the center of the basal plane (Figure 4b).[4]

In the −1B structures, similar to the cavity-free structures, bands originating from the C−C stretching (outer) mode are observed. Notably, the breathing mode band shifts to higher wavenumbers, appearing at 1300 cm^{-1} in *C*222−1B, 1333 cm^{-1} in C114−1B, and 1299 cm^{-1} in C42−1B. This upward shift in the breathing mode band becomes more pronounced in the −7B structures, with the band appearing at 1314 cm^{-1} in *C*222−7B and 1334 cm^{-1} in C114−7B. This shift to higher wavenumbers is attributed to the introduction of a cavity, which disrupts the π-conjugation.[4,29] The variation in breathing mode band positions across different structures can be utilized to identify structural differences by Raman spectroscopy.

In the −7B structures, the C−C stretching (Inner) bands are detected at wavenumbers above 1350 cm^{-1}. This band is not observed in the −1B structures due to the smaller cavity size and resulting steric hindrance.[4] In the −19B structures, the larger cavity size leads to significant disruption of the π-conjugated structure, resulting in the appearance of multiple C−C stretching mode bands. Moreover, The G band intensity is relatively weak in the −0B structure, shows a pronounced increase in the −1B structure, declines again in the −7B structure, and subsequently exhibits a resurgence in the −19B structure.

CONCLUSION

This study presents a comprehensive analysis of the electronic and spectroscopic properties of ACs through density functional theory simulations. By investigating ACs of varying molecular and cavity sizes, it was demonstrated that the electronic properties of ACs can be precisely tuned by adjusting these structural parameters. The XPS spectra showed changes in BEs that corresponded to variations in bandgap, while the Raman spectra revealed specific C−C stretching and breathing modes. Importantly, the addition of cavities caused shifts in the breathing mode, offering valuable information for identifying the structure of ACs using Raman spectroscopy. The results of this research offer a valuable contribution to the field of nanocarbon materials, specifically for the future characterization of synthesized ACs.

METHODS

All density functional theory calculations were carried out using the Gaussian 16 quantum chemistry software package.[30] Structural geometries were optimized at the B3LYP/6-31G(d) level with an ultrafine grid. Following optimization, the XPS and Raman spectra for *C*222, C114, C42, and − *n*B structures were computed, with detailed methodologies provided in the Supporting Information and referenced in our earlier publications.[4,18−23] Normalized XPS spectra were generated through population analysis to determine the electronic energy levels between the HOMO and C 1s, utilizing a software developed by Prof. Yamada.[31,32] The vibrational frequencies for the Raman spectra were derived from the optimized structures and adjusted by a scaling factor of 0.965.[4,23]

ASSOCIATED CONTENT

Supporting Information

The Supporting Information is available free of charge at https://pubs.acs.org/doi/10.1021/acsomega.4c07966.

Supporting Video: vibration modes of Raman spectra (ZIP)

Computational spectroscopy in detail; Raman spectra (0−4000 cm^{-1}); peak assignments of Raman spectra (PDF)

AUTHOR INFORMATION

Corresponding Author

Jungpil Kim − *Carbon & Light Materials Group, Korea Institute of Industrial Technology (KITECH), Jeonju 54853, Republic of Korea;* orcid.org/0000-0003-3663-2774; Phone: +82-63-210-3714; Email: jpkim@kitech.re.kr

Complete contact information is available at: https://pubs.acs.org/10.1021/acsomega.4c07966

Notes

The author declares no competing financial interest.

■ ACKNOWLEDGMENTS

The authors acknowledge the Korea Institute of Science and Technology Information Supercomputing Center for conducting the computational simulations. This work was supported by the Ministry of Trade, Industry, and Energy (MOTIE) [grant no. 20016789].

■ REFERENCES

(1) Di Giovannantonio, M.; Yao, X.; Eimre, K.; Urgel, J. I.; Ruffieux, P.; Pignedoli, C. A.; Müllen, K.; Fasel, R.; Narita, A. Large-Cavity Coronoids with Different Inner and Outer Edge Structures. *J. Am. Chem. Soc.* **2020**, *142*, 12046−12050.

(2) Li, Q.; Zhang, Y.; Xie, Z.; Zhen, Y.; Hu, W.; Dong, H. Polycyclic Aromatic Hydrocarbon-Based Organic Semiconductors: Ring-Closing Synthesis and Optoelectronic Properties. *J. Mater. Chem. C* **2022**, *10*, 2411−2430.

(3) Crasto de Lima, F.; Fazzio, A. Bandgap Evolution in Nanographene Assemblies. *Phys. Chem. Chem. Phys.* **2021**, *23*, 11501−11506.

(4) Park, S.; Jeong, H.; Kim, B.-J.; Lee, Y. K.; Yang, J.; Kim, J. Structural Distinction of Zigzag-Edge Coronoids Analyzed by Spectroscopies. *Carbon* **2023**, *213*, 118248.

(5) Zhu, X.; Liu, Y.; Pu, W.; Liu, F.-Z.; Xue, Z.; Sun, Z.; Yan, K.; Yu, P. On-Surface Synthesis of C144 Hexagonal Coronoid with Zigzag Edges. *ACS Nano* **2022**, *16*, 10600−10607.

(6) Diederich, F.; Staab, H. A. Benzenoid versus Annulenoid Aromaticity: Synthesis and Properties of Kekulene. *Angew. Chem., Int. Ed.* **1978**, *17*, 372−374.

(7) Funhoff, D. J. H.; Staab, H. A. Cyclo[d.e.d.e.e.d.e.d.e.e.]-decakisbenzene, a New Cycloarene. *Angew. Chem., Int. Ed.* **1986**, *25*, 742−744.

(8) Kumar, B.; Viboh, R. L.; Bonifacio, M. C.; Thompson, W. B.; Buttrick, J. C.; Westlake, B. C.; Kim, M.-S.; Zoellner, R. W.; Varganov, S. A.; Mörschel, P.; Teteruk, J.; Schmidt, M. U.; King, B. T. Septulene: The Heptagonal Homologue of Kekulene. *Angew. Chem., Int. Ed.* **2012**, *51*, 12795−12800.

(9) Majewski, M. A.; Hong, Y.; Lis, T.; Gregoliński, J.; Chmielewski, P. J.; Cybińska, J.; Kim, D.; Stępień, M. Octulene: A Hyperbolic Molecular Belt That Binds Chloride Anions. *Angew. Chem., Int. Ed.* **2016**, *55*, 14072−14076.

(10) Beser, U.; Kastler, M.; Maghsoumi, A.; Wagner, M.; Castiglioni, C.; Tommasini, M.; Narita, A.; Feng, X.; Müllen, K. A C216-Nanographene Molecule with Defined Cavity as Extended Coronoid. *J. Am. Chem. Soc.* **2016**, *138*, 4322−4325.

(11) Cyvin, S. J.; Brunvoll, J.; Cyvin, B. N. Enumeration and Classification of Coronoid Hydrocarbons. 10. Double Coronoids. *J. Chem. Inf. Model.* **1990**, *30*, 210−222.

(12) Maghsoumi, A.; Beser, U.; Feng, X.; Narita, A.; Müllen, K.; Castiglioni, C.; Tommasini, M. Raman Spectroscopy of Holey Nanographene C216. *J. Raman Spectrosc.* **2021**, *52*, 2301−2316.

(13) Ma, M. M.; Ding, J. W.; Xu, N. Odd−Even Width Effect on Persistent Current in Zigzag Hexagonal Graphene Rings. *Nanoscale* **2009**, *1*, 387−390.

(14) Zhu, Z.; Wang, D.; Zhang, Z. H.; Qiu, M. Magnetic structures and magnetic device properties of edge-modified armchair-edged graphene nanoribbons. *Carbon* **2016**, *106*, 252−259.

(15) Kim, J.; Yamada, Y.; Fujita, R.; Sato, S. Bromination of Graphene with Pentagonal, Hexagonal Zigzag and Armchair, and Heptagonal Edges. *J. Mater. Sci.* **2015**, *50*, 5183−5190.

(16) Xiang, F.; Maisel, S.; Beniwal, S.; Akhmetov, V.; Ruppenstein, C.; Devarajulu, M.; Dörr, A.; Papaianina, O.; Görling, A.; Amsharov, K. Y.; Maier, S. Planar π-Extended Cycloparaphenylenes Featuring an All-Armchair Edge Topology. *Nat. Chem.* **2022**, *14*, 871−876.

(17) Fang, S.; Hu, Y. H. Open the Door to the Atomic World by Single-Molecule Atomic Force Microscopy. *Matter* **2021**, *4*, 1189−1223.

(18) Kim, J.; Lee, N.; Choi, D.; Kim, D. Y.; Kawai, R.; Yamada, Y. Pentagons and Heptagons on Edges of Graphene Nanoflakes Analyzed by X-ray Photoelectron and Raman Spectroscopy. *J. Phys. Chem. Lett.* **2021**, *12*, 9955−9962.

(19) Kim, J.; Yamada, Y.; Kawai, M.; Tanabe, T.; Sato, S. Spectral Change of Simulated X-ray Photoelectron Spectroscopy from Graphene to Fullerene. *J. Mater. Sci.* **2015**, *50*, 6739−6747.

(20) Kim, J.; Han, J.-W.; Yamada, Y. Heptagons in the Basal Plane of Graphene Nanoflakes Analyzed by Simulated X-ray Photoelectron Spectroscopy. *ACS Omega* **2021**, *6*, 2389−2395.

(21) Kim, J.; Yamada, Y.; Suzuki, Y.; Ciston, J.; Sato, S. Pyrolysis of Epoxidized Fullerenes Analyzed by Spectroscopies. *J. Phys. Chem. C* **2014**, *118*, 7076−7084.

(22) Kim, J.; Lee, N.; Min, Y. H.; Noh, S.; Kim, N.-K.; Jung, S.; Joo, M.; Yamada, Y. Distinguishing Zigzag and Armchair Edges on Graphene Nanoribbons by X-ray Photoelectron and Raman Spectroscopies. *ACS Omega* **2018**, *3*, 17789−17796.

(23) Jeong, H.; Park, S.; Yang, J.; Lee, H.-M.; An, S.; Yamada, Y.; Kim, J. Spectroscopic Distinction of Carbon Nanobelts and Nanohoops. *Carbon* **2023**, *201*, 829−836.

(24) Mori, K.; Kim, J.; Kubo, S.; Yamada, Y. Effects of Molecular Shapes, Molecular Weight, and Types of Edges on Peak Positions of C1s X-ray Photoelectron Spectra of Graphene-Related Materials and Model Compounds. *J. Mater. Sci.* **2022**, *57*, 15789−15808.

(25) Merino-Díez, N.; Garcia-Lekue, A.; Carbonell-Sanromà, E.; Li, J.; Corso, M.; Colazzo, L.; Sedona, F.; Sánchez-Portal, D.; Pascual, J. I.; De Oteyza, D. G. Width-Dependent Band Gap in Armchair Graphene Nanoribbons Reveals Fermi Level Pinning on Au(111). *ACS Nano* **2017**, *11*, 11661−11668.

(26) Moreno, C.; Vilas-Varela, M.; Kretz, B.; Garcia-Lekue, A.; Costache, M. V.; Paradinas, M.; Panighel, M.; Ceballos, G.; Valenzuela, S. O.; Peña, D.; Mugarza, A. Bottom-Up Synthesis of Multifunctional Nanoporous Graphene. *Science* **2018**, *360*, 199−203.

(27) Wang, D.; Zhang, Z.; Zhang, J.; Deng, X.; Fan, Z.; Tang, G. Electronic and Magnetic Properties of Zigzag-Edged Hexagonal Graphene Ring Nanojunctions. *Carbon* **2015**, *94*, 996−1002.

(28) Gordillo Varela, M. A.; Gutiérrez Gómez, G. A.; Chaur Valencia, M. N. A DFT study on Dichloro{(E)-4-dimethylamino-N′-[(pyridin-2 yl)methylidene-κN]benzohydrazide-κO}M2+ (M=Zn, Cu, Ni and Co) complexes: Effect of the metal over association energy and complex geometry. *Rev. Colomb. Quim.* **2016**, *45*, 28−32.

(29) Mapelli, C.; Castiglioni, C.; Zerbi, G.; Müllen, K. Common Force Field for Graphite and Polycyclic Aromatic Hydrocarbons. *Phys. Rev. B* **1999**, *60*, 12710−12725.

(30) Frisch, M.; Trucks, G.; Schlegel, H. B.; Scuseria, G.; Robb, M.; Cheeseman, J.; Scalmani, G.; Barone, V.; Mennucci, B.; Petersson, G. *Gaussian 16*; Gaussian, Inc.: Wallingford CT, 2016. revision B. 01.

(31) Yamada, Y.; Yasuda, H.; Murota, K.; Nakamura, M.; Sodesawa, T.; Sato, S. Analysis of Heat-Treated Graphite Oxide by X-ray Photoelectron Spectroscopy. *J. Mater. Sci.* **2013**, *48*, 8171−8198.

(32) Yamada, Y.; Kim, J.; Matsuo, S.; Sato, S. Nitrogen-Containing Graphene Analyzed by X-ray Photoelectron Spectroscopy. *Carbon* **2014**, *70*, 59−74.

https://doi.org/10.1021/acsomega.4c07966
ACS Omega 2024, 9, 43956−43962